Carbon 205 (2023) 294–301

Contents lists available at ScienceDirect

Carbon

journal homepage: www.elsevier.com/locate/carbon

Dirac cones in graphene grown on a half-filled 4*d*-band transition metal

Antonio J. Martínez-Galera [a,b,*], Haojie Guo [c], Mariano D. Jiménez-Sánchez [c], Enrique G. Michel [b,c,d], José M. Gómez-Rodríguez [b,c,d,1]

[a] Departamento de Física de Materiales, Universidad Autónoma de Madrid, E−28049 Madrid, Spain
[b] Instituto Nicolás Cabrera, Universidad Autónoma de Madrid, E−28049, Madrid, Spain
[c] Departamento de Física de la Materia Condensada, Universidad Autónoma de Madrid, E−28049, Madrid, Spain
[d] Condensed Matter Physics Center (IFIMAC), Universidad Autónoma de Madrid, E−28049, Madrid, Spain

ARTICLE INFO

Keywords:
Graphene
STM
ARPES
XPS
Tunneling height barriers

ABSTRACT

New opportunities for structural and electronic properties engineering of graphene can be achieved by tuning the interfacial interaction, which is ruled by the interplay between *d*-band filling and geometry of the support. Here, is demonstrated the growth of graphene, featuring Dirac cones around the Fermi level, on the rectangular (110) surfaces of Rh, a half-filled 4*d*-band transition metal element. The analysis of the structural properties by low energy electron diffraction (LEED) and scanning tunneling microscopy (STM) shows that domains with a continuum of possible graphene-substrate orientations with angular scatter of around 10° coexist in graphene/Rh (110) surfaces. Within each domain, surface structure is characterized by a distinct stripe-like moiré pattern. The interfacial chemistry analysis, by microprobeX-ray photoelectron spectroscopy (μ-XPS), of all the rotational domains studied, demonstrates the existence of two main levels of interfacial interaction strength, similar to previously reported graphene-metal systems characterized by the absence of Dirac cones around the Fermi level. However, the band structures of these domains probed by micro angle resolved photoelectron spectroscopy (μ-ARPES) present Dirac cones, with Fermi velocities comparable with those previously reported on weakly coupled graphene layers. Both the unique properties of graphene/Rh(110) surfaces and the prospect to obtain novel graphene-metal interfaces through the interplay between *d*-band filling and geometry, are expected to open new opportunities to study phenomena up to now masked behind the interaction with the substrate.

1. Introduction

More than fifteen years after the demonstration of isolated graphene layers [1], the number of substrates that allow a direct growth of this prototypical 2D material is still rather small. The supports that are more frequently used are SiC [2] and few transition metals (TMs) [3,4]. As a matter of fact, the range of metal substrates onto which graphene monolayers preserve its pristine band structure featuring Dirac cones in the vicinity of the Fermi level, is limited to only Ir [5–8], Pt [9], Au [10] and Cu [11,12]. In contrast, 3*d* and 4*d* TMs exhibiting partially-filled *d*-bands, such as Ni [13,14], Rh [15,16], or Ru [15,17,18], generally permit the growth of graphene monolayers with high interfacial hybridization, which results in the destruction of the Dirac cones and the loss of the well-known electronic properties of graphene [13,17,18]. It is due to the fact that in strongly interacting systems, the C-substrate distance appears to be significantly reduced, accompanied by a significant overlapping between the π band and metal states [15]. In these systems with a high interfacial interaction, it is only possible to have Dirac cones around the Fermi level in few layer graphene films grown on the metal support [19].

Beside the *d*-band filling, other key parameter affecting the interaction between graphene and its substrate is the lattice and orientation mismatch. Focusing on graphene monolayers on TMs, the crystallographic relation with the substrate results in the formation of a rich variety of moiré patterns [3,4]. The lattice and orientation mismatch between adlayer and support often determines the formation of large moiré unit cells, where graphene exhibits regular corrugations, that is, periodical modulations of the graphene-metal separation distance [3,4]. Recently, it has been predicted, by geometrical arguments, that the crystallography of the metal substrate, which in turn, determines the geometry of the atomic arrangement of the surface below the graphene layer, could be used to control the corrugation of these periodical

* Corresponding author. Departamento de Física de Materiales, Universidad Autónoma de Madrid, E−28049, Madrid, Spain.
E-mail address: antonio.galera@uam.es (A.J. Martínez-Galera).
[1] Deceased.

https://doi.org/10.1016/j.carbon.2023.01.004
Received 1 June 2022; Received in revised form 12 December 2022; Accepted 5 January 2023
Available online 11 January 2023

modulations [20]. According to that work, in absence of surface reconstructions, while on (111) surfaces of fcc elements, on (110) planes of bcc ones, and on (0001) terminated hcp supports, highly corrugated moiré modulations would be found, on any other low index surfaces, the graphene layer is expected to be rather flat. Consistently, high moiré corrugations have been found on graphene on Rh(111) [15,21], Ru (0001) [15,17], and on Fe(110) [22], whereas rather flat graphene layers have been reported on Cu(001) [23], as well as on Ag(001) [24].

Then, on the basis of all the above mentioned, the interplay between both parameters, *d*-band filling and lattice geometry mismatch, could provide a platform for structural and electronic engineering of graphene. To explore this possibility, the present work is aimed to provide the experimental demonstration of the existence of Dirac cones in the vicinity of the Fermi level on a half-filled 4*d*-band TM by choosing the adequate surface crystallography. In particular, we address the case of graphene grown on (110) surfaces of Rh, a TM with fcc crystal structure. As will be demonstrated below, graphene monolayers are able to keep their Dirac cones close to Fermi level, even in presence of a moderately strong interaction with the Rh(110) substrate. It proves that the crystallographic relation between graphene and a support with non-hexagonal symmetry provides a further means to control the effects of the interfacial interaction strength on the band structure.

2. Experimental

Experiments were performed in two different ultrahigh vacuum (UHV) set-ups. One of them comprises two chambers with independent pumping systems, separated by a gate valve, being one of them employed for sample preparation, which is equipped with a LEED optics for a first quality assessment, and the other for the nanoscale characterization by means of a home-built variable temperature scanning tunneling microscope (VT-STM) [25,26]. The other UHV system was that available at Nanospectroscopy beamline at the Elettra Synchrotron Light Laboratory [27], composed also of one chamber, for sample preparation, and other one, allowing for the characterization by low energy electron microscope (LEEM) and microprobe LEED, XPS and ARPES measurements.

Sample preparation was performed by Ar^+ sputtering at 1 keV of the Rh(110) single crystal, and annealing at 950 °C at an oxygen partial pressure of 2×10^{-6} Torr, followed by annealing to also 950 °C but without supplying O_2. Two different techniques for the growth of graphene were employed. For STM measurements, graphene was grown by (Chemical Vapor Deposition) CVD at an ethylene partial pressure of 3×10^{-7} Torr during 180 s, with the Rh(110) substrate at 900 °C. For microprobe characterization at Nanospectroscopy beamline, the study was focused on single-domain isolated graphene islands grown over the Rh(110) surface, to avoid spurious contributions coming from adjacent flakes displaying different rotational variants. To this end, graphene was grown in a two stages process. First, C atoms were dissolved into the Rh (110) subsurface layers by ethylene exposure at high temperatures. Then, sample was cooled down at lower temperatures, without supplying ethylene, to allow for C segregation towards the surface. This procedure was monitored by LEEM to ensure the growth of isolated micrometer-sized graphene islands scattered over the Rh(110) surface.

STM measurements were performed at the constant current mode with the bias voltage applied to the sample, by using electrochemically etched W tips. STM data acquisition and analysis were performed by using the WSxM software [28]. LEEM measurements were carried out at the bright field mode. In the Nanospectroscopy set-up, the kinetic energy of the, either scattered or emitted electrons, was controlled by a bias voltage (start voltage) applied to the sample. For the acquisition of the spectroscopy data, the kinetic energy of the photoemitted electrons was filtered, with a resolution below 0.3 eV, by means of an electron analyzer with multichannel detector. Microprobe LEED, XPS and ARPES measurements were performed through an aperture of 2 μm diameter.

3. Results and discussion

3.1. Structural characterization of graphene/Rh(110)

Fig. 1 summarizes the main structural features of graphene monolayers grown on Rh(110) surfaces. Specifically, Fig. 1a shows a LEED pattern, which is characterized by a rectangular array of spots, that can be associated to the Rh(110) surface, and six angularly equispaced arcs with identical radii, which can be ascribed to the graphene periodicity (see also a simplified schematic of this pattern in Fig. 1b). In turn, each of these arcs exhibits three intensity maxima placed at equidistant angular positions. For simplicity, the internal structure of these arcs will be described in detail by using, as a reference, the one placed at the top right region of the pattern. As observed, one of its intensity maxima is aligned with the [110] direction of Rh(110), while the others are, respectively, rotated by angles of around $+10°$ and $-10°$ with respect to that crystallographic orientation of the metal substrate. To provide a real space view of the sample, a representative large scale STM image is displayed in Fig. 1c, whose inset shows a STM image, acquired in the region delimited by a black square, exhibiting a quasi-one-dimensional modulation.

The stripe-like superperiodicity, observed in the STM topograph shown in the inset of Fig. 1c, is a moiré pattern associated to the lattice mismatch between graphene and the Rh(110) surface. This geometry of moiré patterns is characteristic of the superposition of the graphene lattice with that of a metal substrate exhibiting an atomic arrangement with either square or rectangular symmetry. This stripe-like geometry has been also observed for graphene monolayers grown on alloys with non-hexagonal unit cells [29]. According to the LEED pattern shown in Fig. 1a, there is coexistence of graphene rotational domains with a continuum of angular orientations between $+10°$ and $-10°$, as referred to the $[1\bar{1}0]$ direction in the reciprocal space of the Rh(110) surface. According to the intensity within the arcs, it is evident, that the predominant rotational variants are those, in which one direction of the atomic lattice of graphene is aligned or nearly aligned, in the reciprocal space, to the $[1\bar{1}0]$ Rh(110) direction, as well as those, in which they exhibit relative angles of around $+10°$ and $-10°$. Note that orientations with angles of the same magnitude but with opposite signs are specular reflections and, hence, correspond to fully equivalent domains. Also, it should be taken into account that a rotation, by a certain angle, of a high symmetry direction of graphene with the $[1\bar{1}0]$ one of Rh in the reciprocal space, corresponds to a rotation angle of the same magnitude with the [001] direction of the metal substrate in the real space.

The atomic scale geometry for orientations around the intensity maxima in LEED patterns, as that shown in Fig. 1a, has been studied, by means of STM, on samples with a partial coverage of graphene to have Rh(110) bare areas as a reference. Fig. 1d shows a STM image acquired on a region around the boundary between a graphene flake (left) and a bare Rh(110) area (right). A stripe-like moiré pattern is observed on the graphene flake. Likewise, on the bare Rh(110) region, the atomic rows along the $[1\bar{1}0]$ direction are resolved. From Fig. 1d it can be inferred that the moiré stripes (see the guidance provided by the yellow arrow) and the $[1\bar{1}0]$ direction of Rh (parallel to the green arrow) are either perpendicular or nearly perpendicular, taking into account the intrinsic uncertainty of RT-STM imaging. Fig. 1e shows a STM image revealing the atomic periodicity of graphene, which appears superimposed to the moiré pattern, in a certain area within the same flake imaged in Fig. 1d. It can be concluded that one of the high symmetry directions of the graphene lattice (black arrow) is either parallel or nearly parallel to the moiré stripes, which, according to Fig. 1d, are, in turn, either perpendicular or nearly perpendicular to the $[1\bar{1}0]$ direction of Rh. In principle, one could think in a unit cell as that indicated by the red parallelogram. Nevertheless, the periodicity of that motif is gradually missing along the direction parallel to the stripes, which is a clear evidence that the superstructure indicated by the red dashed contour is incommensurate, at

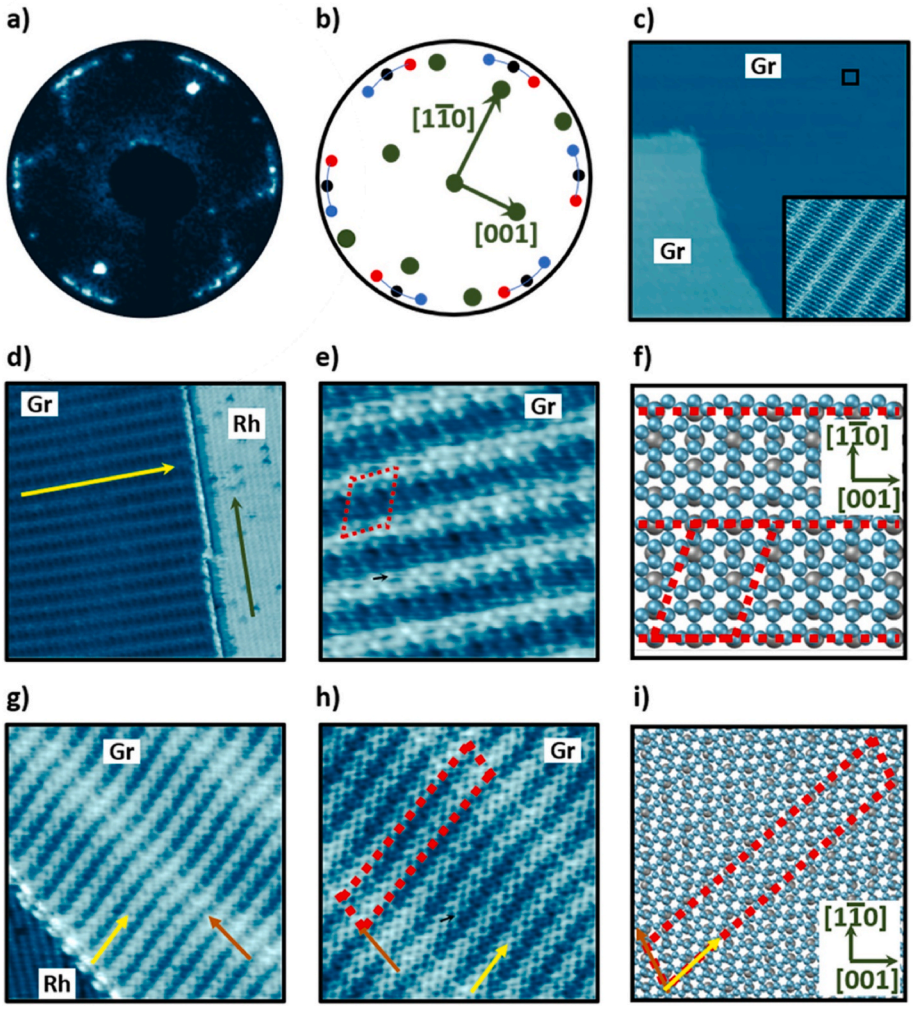

Fig. 1. Structure of graphene monolayers grown on Rh(110). **a)** LEED pattern acquired on a CVD grown graphene monolayer on Rh(110) (electron energy 62 eV). **b)** Schematic of the LEED pattern shown in a). The spots coming from the Rh(110) surface are represented in green, those of the graphene lattice for a relative angle of 0° with respect to the Rh [1$\bar{1}$0] direction, in black, and those, associated to a relative angle of around 10° between the graphene lattice and the Rh [1$\bar{1}$0] direction, in red (its specular reflection is represented in blue). The arcs connecting these three spots represent the continuum of possible orientations of the graphene layer with respect to the Rh(110) surface. **c)** Large scale STM image of graphene grown on Rh(110). Inset: STM topograph acquired in the area indicated by the black square. **d)** STM image simultaneously resolving both, a fraction of a graphene flake with a relative orientation of around 0° as referred to the [001] substrate direction, and a region of the Rh(110) surface in its vicinity. **e)** Atomically resolved STM image, acquired on a region of the same graphene flake imaged in Fig. 1d **f)** Tentative schematic representation of the atomic registry of C atoms over the Rh(110) surface for that rotational domain. **g)** STM image acquired at the boundary of a graphene flake and the Rh(110) surface in the surroundings, with a relative rotation between the atomic lattices of both of around 10°, as referred to the Rh[001] direction. **h)** Atomically resolved STM image acquired on a region of that rotational variant. The red dashed parallelogram indicates a possible unit cell. **i)** Tentative schematic of the atomic positioning of graphene over the Rh(110) surface for that rotational domain. The red dashed parallelograms displayed in f) and i) indicate nearly coincident structures, which could be an approximation of the actual atomic arrangements of both rotational variants. In f) and i), C atoms of the graphene layer are represented by blue spheres and those of the Rh(110) surface by grey ones. The moiré stripes are indicated by red dashed lines. Tunneling parameters: c) $I_T = 0.7$ nA, $V_s = +0.42$ V; size: 400 × 400 nm^2. Inset: $I_T = 1.7$ nA, $V_s = +0.32$ V; size: 20 × 20 nm^2. d) $I_T = 8.1$ nA, $V_s = +1.0$ V; size: 15 × 15 nm^2. e) $I_T = 8.1$ nA, $V_s = +1.0$ V; size: 5 × 5 nm^2. g) $I_T = 1.0$ nA, $V_s = +1.0$ V; size: 10 × 10 nm^2. h) $I_T = 2.9$ nA, $V_s = +1.0$ V; size: 7 × 7 nm^2. (A colour version of this figure can be viewed online.)

least along that direction.

On the basis of these experimental findings, a schematic representation of a plausible atomic arrangement for the rotational variant analyzed in Fig. 1d and e, is proposed in Fig. 1f. According to this schematic, the superposition of the Rh(110) lattice and that of graphene with a relative angle of exactly 0°, as referred to the [001] Rh direction, would reproduce fairly well the measured structural parameters. Based on it, the moiré fringes would be separated by ~1.08 nm, roughly matching with four times the atomic spacing of the Rh substrate along the [1$\bar{1}$0] direction. This atomic registry would imply that the atomic periodicity of graphene must be increased by ~2.4%. Under these conditions, the incommensurate structure indicated in Fig. 1f, by the red dashed parallelogram, would be consistent with that experimentally observed in STM images (see Fig. 1e). It is, however, noteworthy to mention that, almost identical incommensurate structures would be obtained not only for a rotation angle of exactly 0°, as represented in Fig. 1f, but also for any small angle of a high symmetry direction of the graphene lattice with respect to the [001] direction of Rh.

Fig. 1g shows a STM image acquired around the edge of a graphene flake, where the atomic rows along the [1$\bar{1}$0] direction in the adjoining Rh(110) bare area are clearly resolved. As observed, the resulting moiré pattern is rather complex, and two kinds of features can be distinguished. On the one hand, there is a set of equispaced stripes, which are not straight, but they exhibit a periodic or nearly periodic modulation. One of these stripes is indicated in Fig. 1g by a yellow arrow. On the other hand, there is also another set of stripes with a larger separation. One of them is indicated in Fig. 1g by a brown arrow. The angle between these stripes with larger separation and the atomic rows along the [1$\bar{1}$0] Rh(110) direction is ~27°. Fig. 1h displays a STM image acquired on a region, within the same flake observed in Fig. 1g, where the atomic periodicity of the graphene structure (black arrow) is observed together with the two kinds of stripes (indicated by yellow and brown arrows) comprising the moiré pattern. The angle between the stripes with larger/shorter separation and one of the high symmetry directions of the graphene atomic structure is ~14°/26°. According to the image, the red dashed parallelogram, with lateral dimensions of around 5.5 and 0.9 nm, could be a possible unit cell.

From the STM images shown in Fig. 1g and h a schematic representation of a plausible atomic arrangement for this rotational variant is presented in Fig. 1i. The superposition of the graphene lattice and that of the Rh(110) surface, under a relative orientation between one of the high symmetry directions of the former and the [001] one of the latter of

around 9.3°, results in a nearly commensurate superstructure (see the red dashed parallelogram). This nearly coincidence of the atomic networks of graphene and of the Rh(110) support would require that the lattice of the former to be expanded by ~ 2%. The length of the shorter side of this nearly commensurate structure is 0.9 nm and it is rotated with respect to the Rh [1$\bar{1}$0] direction by 25.2° and with the graphene lattice by 14.1°. The length of the larger side is of 5.6 nm, and the rotation angle between both sides is of 73.1°. The larger side is rotated with respect to the Rh [1$\bar{1}$0] direction by 48° and with the graphene lattice by 27.3°, in good agreement with the experimental values.

3.2. Interfacial chemistry characterization of graphene/Rh(110)

In the previous paragraphs, the structure of graphene monolayers epitaxially grown on Rh(110) surfaces has been analyzed, having demonstrated that the graphene lattice can adopt any orientation relative to the substrate with angles between 0° and ~±10°, as referred to the [001] ([1$\bar{1}$0] in the reciprocal space) direction of Rh(110), being predominant orientations of around 0 and ± 10°. Next, a detailed microprobe XPS study of the bonding chemistry at the graphene/Rh(110) interface will be provided, analyzing possible differences between different orientations. Fig. 2a–c shows LEEM images, displaying single domain graphene islands grown on Rh(110) surfaces. Within each image, the specific island employed for the XPS characterization is indicated by a red arrow. Fig. 2d collects C1s XPS spectra acquired on the respective island of each image. As observed, these spectra exhibit important common features, since each of them can be deconvoluted into three components with binding energies of 283.6, 284.4 and 284.9 eV, which are plotted in green, blue and red, respectively. The two components with higher binding energies dominate these spectra, while the presence of the other one (green traces) is nearly residual.

Because for each C atom within the moiré structure the chemical environment is different, the fitting model proposed in Fig. 2, with only three components, is an oversimplification, although it allows to obtain a qualitative view. Specifically, the splitting of the C1s spectra into various components could be ascribed to different degrees of C hybridization over the Rh(110) surface. The component with the smallest binding energy, whose contribution to the spectra is nearly marginal in the majority of the cases, was found to present a variable intensity during the experiments (see subheadings A2 and A3 in the supplementary information). C1s components in XP spectra with similar binding energies have been previously reported for different carbides on metal surfaces [7,22,30,31]. Hence, in the present case, this component could be associated to the presence of an almost residual amount of carbidic C trapped under the graphene layer, and/or to C chemisorbed to the Rh (110) surface in the vicinity of the flakes, as well as, dissolved into the first subsurface layers below the flakes and their surroundings. The other two components confer the spectra an overall appearance, exhibiting a good accordance with previously reported spectra, acquired on various metal supported graphene monolayers, with highly differentiated chemical environments for C atoms [15]. Interestingly, the binding energies of both components exactly coincide with these of their counterparts in the spectrum reported for the graphene/Rh(111) interface, by Preobrajenski et al., which were interpreted by these authors as the result of differences in interfacial orbital mixing between moiré subregions with different graphene-metal distances [15]. A similar splitting into two components was also reported for graphene monolayers grown on Ru(0001) surfaces, which were interpreted by these authors also as the result of the coexistence of two clearly distinguished degrees of interfacial interaction between C and Ru [15]. Therefore, the two components with binding energies of 284.4 and 284.9 eV observed in the XP spectra, acquired in the present work, could be associated to C atoms with different orbital mixing with atoms in the Rh(110) surface below. Consistently, a C1s component with a binding energy of also 284.9 eV has been previously reported for sp^3 diamond-like C [32]. Also, there is a dominant component at the very same binding energy in spectra previously obtained for graphene/Fe(110) and graphene/Ni (111), for which a strongly graphene-substrate interaction was reported [22]. Likewise, the energy positioning of the other component in the spectra shown in Fig. 2d, is closer to that of the single component in the spectra previously reported for graphitic C [15]. It could imply that C

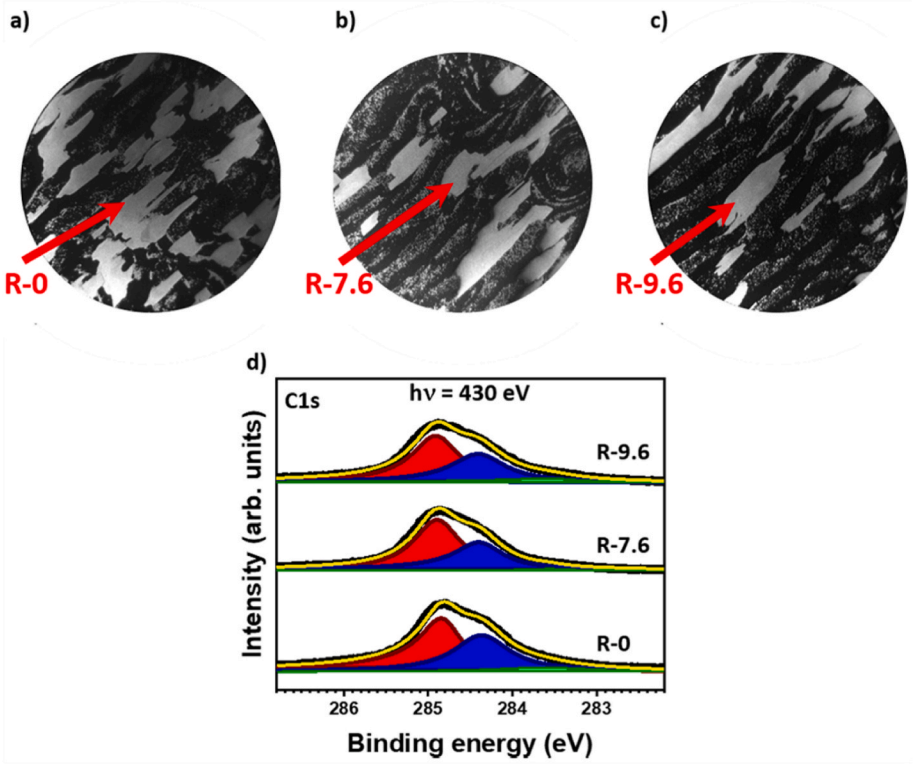

Fig. 2. XPS study of the graphene/Rh(110) surface. **a)-c)** Bright field LEEM images showing the graphene islands (indicated by red arrows) on which the respective XP spectra shown in the lower panel were acquired. The field of view of the three images was 20 μm and the acquisition electron energy 16 eV. **d)** C1s XP spectra acquired with a photon energy of 430 eV on the flakes, indicated in the upper panels, with relative angles of 0°, 7.6° and 9.6° between the graphene lattice and the [001] direction of the Rh(110) surface beneath. The experimental points are represented in black, while the red, blue and green traces represent the three components, with respective binding energies of 284.9, 284.4 and 283.6 eV, giving rise to the fit trace represented in yellow. (A colour version of this figure can be viewed online.)

atoms giving rise to the component with higher binding energy in the spectra shown in Fig. 2d, would present a stronger chemisorption to the Rh(110) surface than those responsible for that at 284.4 eV. To finish with the issue of the interfacial chemistry, as observed in Fig. 2d, there are significant similarities between the C1s spectra acquired on flakes with relative orientations of 0°, 7.6° and 9.6° of a high symmetry direction of the graphene lattice with respect to the [001] substrate direction. For this reason, similar bonding chemistries are qualitatively expected in these rotational variants.

It is interesting to pay attention to the mentioned similitude between the C1s spectra acquired on graphene on rectangular Rh(110) surfaces, with these measured when a Rh(111) surface with hexagonal symmetry is employed as a support. It suggests that although substrate symmetry decides the spatial distribution of the moiré subregions, this configurational parameter of the support would not play, at least in this case, a significant role in the overall degrees of interfacial orbital overlapping. Thus, the XPS data summarized in Fig. 2 suggest that the interfacial chemistry of graphene/Rh(110) must be somehow analogous to that of graphene/Rh(111), despite the different symmetry of the metal supports. However, the typically measured apparent corrugations on both graphene/metal systems are markedly different, being significantly smaller for graphene grown on the rectangular Rh(110) surfaces. It suggests that the existence of two marked levels of hybridization does not necessarily implies a high interfacial corrugation.

3.3. *dI/dz mapping on graphene/Rh(110)*

The possible correlation between the two levels of orbital mixing at the interface, evidenced by XPS measurements, and the differences in the graphene-metal distances, arising from the moiré patterns, has been investigated by means of STM barrier height mapping. These maps have been obtained by applying a modulation to the *z* piezo (typically 40–60 pm peak to peak) of high frequencies compared to the feedback loop response, but below the low-pass filter cut-off integrated in the STM preamplifier. The resulting variations in the tunneling current were registered by a lock-in amplifier, whose output was connected to one input channel of the digital signal processor governing the operation of the STM. Simultaneously to the acquisition of the d*I*/d*z* maps, the corresponding topography image has been also obtained in the same sample region. Fig. 3a shows a STM topography image acquired on a region of graphene grown on Rh(110). Fig. 3b displays a d*I*/d*z* map acquired together with the STM image shown in Fig. 3a. A periodic modulation in registry with the moiré stripes, observed in the STM topograph (Fig. 3a), is present in the d*I*/d*z* maps (Fig. 3b). To guide the eye, a red arrow is shown over one of the stripes observed.

Similarly, Fig. 3e shows a d*I*/d*z* map, acquired simultaneously to the STM image shown in Fig. 3d, where a different moiré pattern from that associated to the rotational variant analyzed in Fig. 3a–c, is resolved. As indicated by the red and yellow arrows, the tunneling barrier map shown in Fig. 3e exhibits a stripe-like pattern correlated with the moiré periodicity (compare to topograph observed in Fig. 3d).

An essential issue to allow for a correct interpretation of STM barrier height maps is that they result from local variations of both the interfacial chemistry and the geometry [33,34]. The geometric component influencing these maps arises, mainly, from the misalignment between the direction of the modulation, applied to the *z* piezo, and the local normal surface vector in each point of the scanning area [34]. It was reported that this geometric contribution, in each point of STM barrier height maps, is related to the cosine of the angle between the modulation direction and the vector normal to the surface at that point [34]. To this end, the cosine of the angle between the modulation direction, which is parallel to the *z* axis, and the gradient vector of the surface in each point, as obtained using as approximation the geometry given by the STM topography image displayed in Fig. 3a, is represented in Fig. 3c. Accordingly, the corresponding cosine map extracted from the topography image shown in Fig. 3d is provided in Fig. 3f. As observed in both data sets, the brighter/darker areas across the fringes observed in the respective cosine maps match also the brighter/darker ones in the corresponding STM barrier maps shown in Fig. 3b,e. Then, a possible interpretation could be that the local variations observed in the STM barrier maps shown in Fig. 3b,e could be, at some extent, induced by geometric contributions rather than by local variations in the interfacial chemistry across the moiré stripes. Nevertheless, one could argue that significant differences in the bonding chemistry across the moiré fringes could still exist, having certain influence on the STM barrier height maps together with the contribution associated to geometrical issues. It would

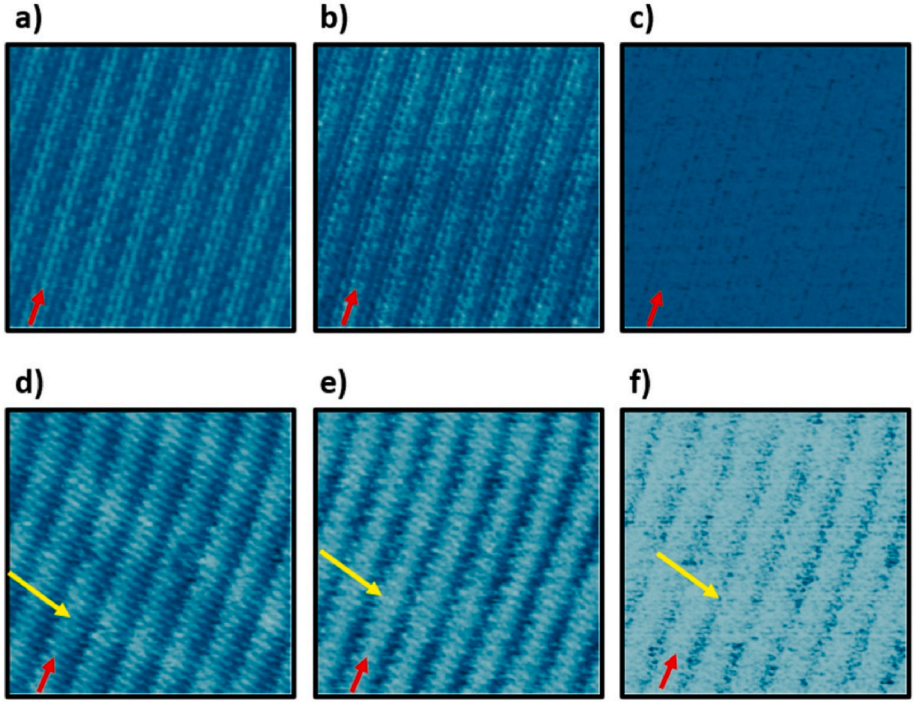

Fig. 3. Tunneling barrier height study on graphene monolayers grown on Rh(110). **a)** STM topograph and **b)** d*I*/d*z* map, simultaneously acquired on the same region of graphene grown on Rh(110). **c)** Map of the cosine of the angle between the modulation direction and the gradient vector of the surface in each point of the STM image displayed in Fig. 3a. Red arrows indicate the direction of the moiré stripes. **d), e), f)** Respective STM topograph, d*I*/d*z* map and cosine map for a rotational variant different from that analyzed in Fig. 3a–c. Red and yellow arrows indicate the direction of the moiré stripes. Lock-in parameters: b) Modulation frequency: 3.2 kHz; Modulation amplitude: 57 pm peak to peak; e) Modulation frequency: 3.2 kHz, Modulation amplitude: 45 pm peak to peak. Tunneling parameters: a) $I_T = 1.2$ nA, $V_s = +0.18$ V; d) $I_T = 1.1$ nA, $V_s = +0.16$ V. Size: 9.6 × 9.6 nm^2 for all the panels. (A colour version of this figure can be viewed online.)

be consistent with the existence of two degrees of interfacial orbital overlapping suggested by the XPS study. Work function variations across moiré patterns, have been previously reported for graphene monolayers grown on various metal substrates as Pt(111) [35,36], Ir(111) [37], and Ru(0001) [38], by means of STM barrier height maps and, also, of single *I-z* curves. However, for none of these works the above mentioned geometric issues were taken into account.

3.4. Band structure of graphene/Rh(110)

Following the study, at the nanoscale, of graphene monolayers epitaxially grown on Rh(110) surfaces through tunneling barrier height maps, provided in the previous paragraphs, the electronic properties of this system will be analyzed from the perspective offered by μ-ARPES. Fig. 4 shows the band structures obtained for two rotational variants denoted as R-0 and R-9.6, corresponding to graphene-substrate orientations around the two non-equivalent intensity maxima observed in LEED patterns (see also Fig. 1a), projected along the K′-K direction connecting opposite sites of the first Brillouin Zone. Additionally, to provide a wider perspective, the band structure, obtained for the R-7.6 rotational variant, with an intermediate graphene-substrate angular orientation, is also provided. According to previous works, the diffuse background featured in the respective three LEED patterns could be a signature of a high structural quality of the graphene flakes [39,40]. As observed, the three band structures, projected along the above mentioned direction in the reciprocal space (see also the second column in Fig. 4) exhibit the characteristic linear dispersion of graphene around the K and K′ points. In all the three cases, a change in the slope of the projected dispersion relationship of graphene is found at the crossing points with the 4*d* band of the Rh(110) surface. The Fermi velocities, as extracted from the projected band structure above/below the crossing points with the 4*d* band of the Rh(110) substrate, are of $(1.3 \pm 0.3) \times 10^{-6}/(1.1 \pm 0.2) \times 10^{-6}$, $(1.4 \pm 0.3) \times 10^{-6}/(1.2 \pm 0.2) \times 10^{-6}$ and $(1.4 \pm 0.3) \times 10^{-6}/(1.2 \pm 0.2) \times 10^{-6}$ m/s, respectively, for the R-0, R-7.6 and R-9.6 rotational variants. These values have been obtained by fitting the energy versus the *k* value for which the intensity is maximum for each value of the energy. For these three rotational domains, the respective band structures evidence graphene doping. The subheading A1 in the supplementary information shows the band structures of these rotational variants projected along a different direction in the reciprocal space. Moreover, the subheadings A2 and A3 show the complete analysis of other different rotational variants. As a reference to allow for a better interpretation of the ARPES data, the experimental Rh(110) bands are provided, which are comparable with previous experiments [41]. A direct identification is not however possible due to the different experimental parameters. The Rh(110) bands are then identified by comparison with the expected Fermi surface contour [42] and theoretical calculations [43].

Fig. 4 demonstrates the coexistence of rotational domains, whose band structures present Dirac cones, in graphene monolayers grown on Rh(110) surfaces (see also Figs. A1 and A3 in the supplementary information). This is the first graphene-metal system, reported till now, with a support being a metal with the *d* band only half-filled, and different than a 5*d* transition one, for which Dirac cones are found at the vicinity of the Fermi level, without decoupling by intercalation of species at the interface. Even more, the Dirac cones observed for the three rotational variants analyzed in Fig. 4, although they are shifted with respect to the Fermi level, and mildly distorted at the crossing points with the *d* band of Rh, evidencing weak hybridization, they are characterized by Fermi velocities comparable to those reported on weakly coupled graphene

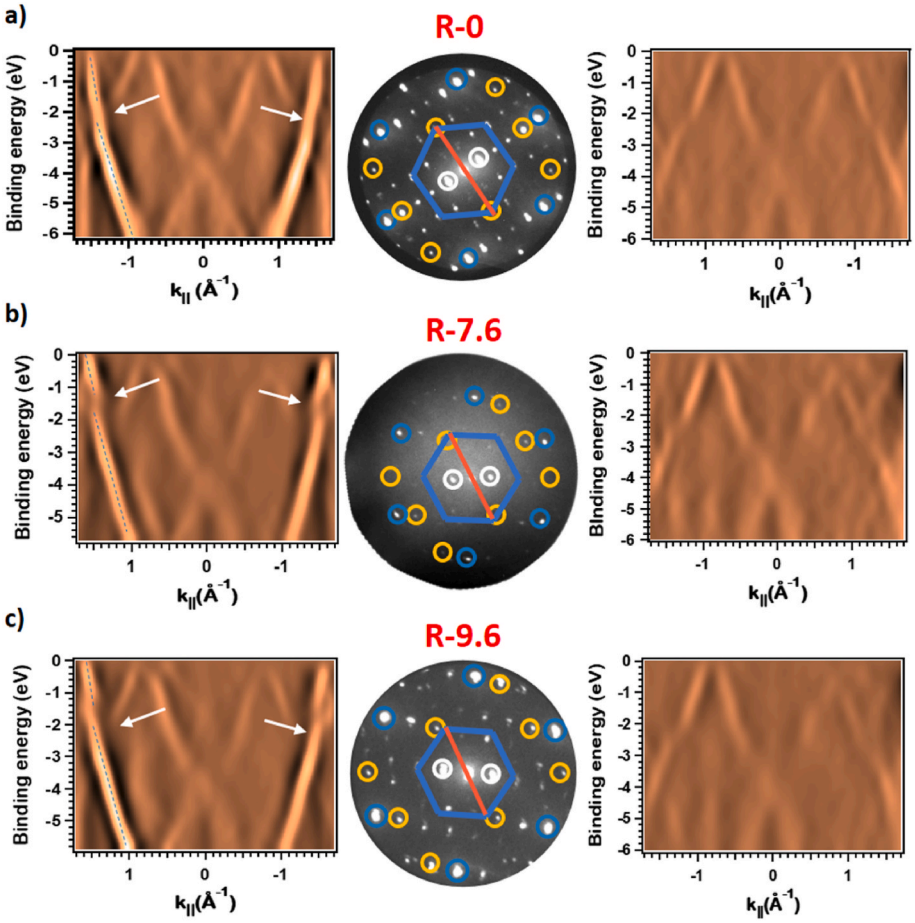

Fig. 4. ARPES spectra acquired at a photon energy of 120 eV on the graphene flakes indicated in Fig. 2a–c **a)**, **b)** and **c)** Band structures of the R-0, R-7.6 and R-9.6 domains (left column), projected along the reciprocal space directions indicated by the red line in the respective LEED patterns acquired at 45 eV (second column). Light blue dashed lines indicate the projection of the Dirac cones above and below the crossing with the *d* band of Rh. The crossings between π bands of graphene and the *d* band of Rh are indicated by white arrows. In the LEED patterns, the spots associated to the periodicity of the underlying Rh (110) surface are encircled in orange, these of the graphene periodicity in blue, these of the periodicity of the moiré stripes in white, and the first Brillouin Zone of graphene is indicated by a blue hexagon. As a reference, the third column shows the band structure of the pristine Rh(110) surface, projected along the same directions in the reciprocal space as these indicated in the second column when the graphene layer is placed on top. This set of ARPES measurements was acquired in exactly the same sample locations as the XPS spectra shown in Fig. 2. (A colour version of this figure can be viewed online.)

systems [9,12,44–47]. In fact, the Fermi velocities extracted from the projected band structures above the crossing points with the 4*d* band of Rh are between the highest reported to date in graphene. The existence of band structures featuring Dirac cones at the vicinity of the Fermi level is, in principle, rather surprising for substrates of Rh, which is a 4*d* TM with the *d* band half-filled. Here is noteworthy to mention that, in analogy with the *d* band model, employed to predict trends in the binding of molecular adsorbates on metal surfaces [48], the graphene-metal interaction tends to be stronger for 3*d* and 4*d* TMs with the *d* bands half-filled than for 5*d* ones [3]. Indeed, they have been proven to give rise to graphene adlayers showing significant chemisorption, which are generally characterized by the absence of Dirac cones near the Fermi level [3,4]. In the case of Rh, previous works have demonstrated that the π band of epitaxial graphene on Rh(111) surfaces, is strongly hybridized with the *d* band of the metal substrate [15,16,21]. Thus, the crystallographic orientation of the underlying metal surface seems to play a decisive role in the electronic properties of the graphene layer grown on top. A plausible explanation is based on the fact that the interfacial bonding landscape must depend on geometrical concerns as lattice parameter and symmetry mismatches. In this regard, on most hexagonal surfaces, which exhibit a symmetry matching with the atomic arrangement of graphene, the resulting moiré superstructures can be subdivided into different subregions with a certain spatial extension. Around the central part of each of these moiré subdivisions, the atomic lattices of graphene and support are somehow nearly coincident, giving rise to a specific atomic registry, which is different from that of the other subdivisions. However, that nearly coincidence of the atomic lattices is not possible for supports with non-hexagonal atomic packing, which is translated into rather different spatial distributions of the interfacial chemistry. Thus, on the basis of the experimental results summarized in Fig. 4, these differences could play a decisive role in the band structure.

4. Conclusion

Here, the first graphene monolayers, grown on a half-filled 4*d* band TM, with band structure featuring Dirac cones at the vicinity of the Fermi level, are reported. This success has provided a deeper view of the graphene-metal interaction, highlighting that the interplay, between *d* band filling and geometry of the support, affects the properties of the 2D material supported on it. From the structural point of view, the graphene/Rh(110) surface is characterized by the coexistence of domains, whose possible graphene-substrate orientations lie within a continuum between 0° and 10° as referred to the [001] direction of Rh, being preferred, orientations around the ends of that angular interval. STM images have demonstrated that these domains exhibit quasi one-dimensional stripe-like moiré patterns. From a chemical point of view, the analysis by μ-XPS has demonstrated that, within these moiré superstructures, there are mainly two different degrees of interfacial orbital mixing. It is similar to what was previously reported for various strongly interacting graphene monolayers with metal substrates, being generally characterized by the absence of Dirac cones around the Fermi level. Nevertheless, the electronic structure of graphene/Rh(110) surfaces as probed by μ-ARPES, is characterized by Dirac cones with Fermi velocities between the highest measured on weakly coupled graphene systems. It demonstrates that the marked differences in the interfacial chemistry within each moiré pattern, revealed by XPS, do not necessarily imply chemisorption involving the absence of Dirac cones in the vicinity of the Fermi level, which is opposite to what was previously believed. The combination of an interfacial chemistry characterized by essentially two degrees of orbital intermixing, an electronic structure dominated by the presence of Dirac cones around the Fermi level, as well as a relatively low corrugation makes the graphene/Rh(110) surface a unique system. It demonstrates that the interplay between *d*-band filling and geometry of the atomic arrangement of the metal substrate, can be exploited for graphene engineering.

CRediT authorship contribution statement

Antonio J. Martínez-Galera: Investigation, Methodology, Conceptualization, Formal analysis, Visualization, Writing – review & editing, Validation, Project administration, Funding acquisition. **Haojie Guo:** Investigation. **Mariano D. Jiménez-Sánchez:** Investigation. **Enrique G. Michel:** Methodology, Conceptualization, Formal analysis, Writing – review & editing, Validation. **José M. Gómez-Rodríguez:** Methodology, Conceptualization, Formal analysis, Writing – review & editing, Validation, Project administration, Funding acquisition.

Declaration of competing interest

The authors declare that they have no known competing financial interests or personal relationships that could have appeared to influence the work reported in this paper.

Acknowledgment

The authors dedicate this work to the memory of Prof. José María Gómez Rodríguez, personal friend, mentor and colleague. The authors acknowledge the support from the staff of Nanospectroscopy beamline at Elettra Synchrotron Light Laboratory. Financial support from the Spanish MINECO under project MAT2016-77852-C2-2-R, from the "María de Maeztu" program for units of excellence in R&D (grant number CEX2018-000805-M) is gratefully acknowledged. A. J. M.-G. acknowledges funding from the Spanish MICINN through Project No. PID2020-116619 GA-C22, and from the Comunidad de Madrid and the Universidad Autónoma de Madrid through project SI3/PJI/2021-00500. E. G. M. acknowledges funding from the Spanish MICINN through Project No. PID2021-123295NB-I00. The research leading to this result has been supported by the project CALIPSOplus under Grant Agreement 730872 from the EU Framework Programme for Research and Innovation HORIZON 2020.

Appendix A. Supplementary data

Supplementary data to this article can be found online at https://doi.org/10.1016/j.carbon.2023.01.004.

References

[1] K.S. Novoselov, A.K. Geim, S.V. Morozov, D. Jiang, Y. Zhang, S.V. Dubonos, et al., Electric field effect in atomically thin carbon films, Science 306 (2004) 666–669.
[2] C. Berger, Z.M. Song, T.B. Li, X.B. Li, A.Y. Ogbazghi, R. Feng, et al., Ultrathin epitaxial graphite: 2D electron gas properties and a route toward graphene-based nanoelectronics, J. Phys. Chem. B 108 (2004) 19912–19916.
[3] J. Wintterlin, M.L. Bocquet, Graphene on metal surfaces, Surf. Sci. 603 (2009) 1841–1852.
[4] M. Batzill, The surface science of graphene: metal interfaces, CVD synthesis, nanoribbons, chemical modifications, and defects, Surf. Sci. Rep. 67 (2012) 83–115.
[5] I. Pletikosic, M. Kralj, P. Pervan, R. Brako, J. Coraux, A.T. N'Diaye, et al., Dirac cones and minigaps for graphene on Ir(111), Phys. Rev. Lett. 102 (2009), 056808.
[6] S. Rusponi, M. Papagno, P. Moras, S. Vlaic, M. Etzkorn, P.M. Sheverdyaeva, et al., Highly anisotropic Dirac cones in epitaxial graphene modulated by an island superlattice, Phys. Rev. Lett. 105 (2010), 246803.
[7] C. Herbig, T. Knispel, S. Simon, U.A. Schroder, A.J. Martinez-Galera, M.A. Arman, et al., From permeation to cluster arrays: graphene on Ir(111) exposed to carbon vapor, Nano Lett. 17 (2017) 3105–3112.
[8] F. Huttmann, D. Klar, N. Atodiresei, C. Schmitz-Antoniak, A. Smekhova, A. J. Martinez-Galera, et al., Magnetism in a graphene-4 f-3d hybrid system, Phys. Rev. B 95 (2017).
[9] P. Sutter, J.T. Sadowski, E. Sutter, Graphene on Pt(111): growth and substrate interaction, Phys. Rev. B 80 (2009), 245411.
[10] J.M. Wofford, E. Starodub, A.L. Walter, S. Nie, A. Bostwick, N.C. Bartelt, et al., Extraordinary epitaxial alignment of graphene islands on Au(111), New J. Phys. 14 (2012), 053008.
[11] A.L. Walter, S. Nie, A. Bostwick, K.S. Kim, L. Moreschini, Y.J. Chang, et al., Electronic structure of graphene on single-crystal copper substrates, Phys. Rev. B 84 (2011), 195443.

[12] S. Gottardi, K. Muller, L. Bignardi, J.C. Moreno-Lopez, P. Tuan Anh, O. Ivashenko, et al., Comparing graphene growth on Cu(111) versus oxidized Cu(111), Nano Lett. 15 (2015) 917–922.
[13] A. Varykhalov, J. Sanchez-Barriga, A.M. Shikin, C. Biswas, E. Vescovo, A. Rybkin, et al., Electronic and magnetic properties of quasifreestanding graphene on Ni, Phys. Rev. Lett. 101 (2008), 157601.
[14] A. Nagashima, N. Tejima, C. Oshima, Electronic states of the pristine and alkali-metal-intercalated monolayer graphite/Ni(111) systems, Phys. Rev. B 50 (1994) 17487–17495.
[15] A.B. Preobrajenski, M.L. Ng, A.S. Vinogradov, N. Martensson, Controlling graphene corrugation on lattice-mismatched substrates, Phys. Rev. B 78 (2008), 073401.
[16] M. Fonin, M. Sicot, O. Zander, S. Bouvron, P. Leicht, U. Rüdiger, et al., Spatial corrugation and bonding of single layer graphene on Rh(111), arXiv:1010.1389v1 [cond-mat.mtrl-sci], 2010.
[17] T. Brugger, S. Gunther, B. Wang, J.H. Dil, M.L. Bocquet, J. Osterwalder, et al., Comparison of electronic structure and template function of single-layer graphene and a hexagonal boron nitride nanomesh on Ru(0001), Phys. Rev. B 79 (2009), 045407.
[18] C. Enderlein, Y.S. Kim, A. Bostwick, E. Rotenberg, K. Horn, The formation of an energy gap in graphene on ruthenium by controlling the interface, New J. Phys. 12 (2010), 033014.
[19] A. Kordatos, N. Kelaidis, S.A. Giamini, J. Marquez-Velasco, E. Xenogiannopoulou, P. Tsipas, et al., AB stacked few layer graphene growth by chemical vapor deposition on single crystal Rh(111) and electronic structure characterization, Appl. Surf. Sci. 369 (2016) 251–256.
[20] A.J. Martínez-Galera, J.M. Gómez-Rodríguez, Influence of metal support in-plane symmetry on the corrugation of hexagonal boron nitride and graphene monolayers, Nano Res 11 (2018) 4643–4653.
[21] A. Martin-Recio, C. Romero-Muniz, A.J. Martinez-Galera, P. Pou, R. Perez, J. M. Gomez-Rodriguez, Tug-of-war between corrugation and binding energy: revealing the formation of multiple moire patterns on a strongly interacting graphene-metal system, Nanoscale 7 (2015) 11300–11309.
[22] N.A. Vinogradov, A.A. Zakharov, V. Kocevski, J. Rusz, K.A. Simonov, O. Eriksson, et al., Formation and structure of graphene waves on Fe(110), Phys. Rev. Lett. 109 (2012), 026101.
[23] H.I. Rasool, E.B. Song, M. Mecklenburg, B.C. Regan, K.L. Wang, B.H. Weiller, et al., Atomic-scale characterization of graphene grown on copper (100) single crystals, J. Am. Chem. Soc. 133 (2011) 12536–12543.
[24] S. Grandthyll, K. Jacobs, F. Muller, Liquid-source growth of graphene on Ag(001), Phys. Status Solidi B 252 (2015) 1695–1699.
[25] O. Custance, S. Brochard, I. Brihuega, E. Artacho, J.M. Soler, A.M. Baró, et al., Single adatom adsorption and diffusion on Si(111)-(7x7) surfaces: scanning tunneling microscopy and first-principles calculations, Phys. Rev. B 67 (2003), 235410.
[26] A.J. Martinez-Galera, J.M. Gomez-Rodriguez, Nucleation and growth of the prototype azabenzene 1,3,5-triazine on graphite surfaces at low temperatures, J. Phys. Chem. C 115 (2011) 11089–11094.
[27] A. Locatelli, L. Aballe, T.O. Mentes, M. Kiskinova, E. Bauer, Photoemission electron microscopy with chemical sensitivity: SPELEEM methods and applications, Surf. Interface Anal. 38 (2006) 1554–1557.
[28] I. Horcas, R. Fernandez, J.M. Gomez-Rodriguez, J. Colchero, J. Gomez-Herrero, A. M. Baro, WSXM: a software for scanning probe microscopy and a tool for nanotechnology, Rev. Sci. Instrum. 78 (2007), 013705.
[29] V. Uhlir, F. Pressacco, J.A. Arregi, P. Prochazka, S. Prusa, M. Potocek, et al., Single-layer graphene on epitaxial FeRh thin films, Appl. Surf. Sci. 514 (2020).
[30] S. Rey, F. Le Normand, Surface transformations of carbon (graphene, graphite, diamond, carbide), deposited on polycrystalline nickel by hot filaments chemical vapour deposition, Thin Solid Films 519 (2011) 4426–4428.
[31] E. Papastavros, P.J. Shea, M.A. Langell, Oxygen, carbon, and sulfur segregation in annealed and unannealed zerovalent iron substrates, Langmuir 20 (2004) 11509–11516.
[32] A. Chavanne, J.C. Arnault, J. Barjon, J. Arabski, Bias-enhanced nucleation of diamond on iridium: a comprehensive study of the first stages by sequential surface analysis, Surf. Sci. 605 (2011) 564–569.
[33] R. Schuster, J.V. Barth, J. Wintterlin, R.J. Behm, G. Ertl, Distance dependence and corrugation in barrier-height measurements on metal-surfaces, Ultramicroscopy 42 (1992) 533–540.
[34] J.M. Gomez-Rodriguez, J. Gomez-Herrero, A.M. Baro, Imaging cos(s, z) - a method to separate the geometric and compositional contributions on STM barrier height profiles, Surf. Sci. 220 (1989) 152–164.
[35] M. Sasaki, Y. Yamada, Y. Ogiwara, S. Yagyu, S. Yamamoto, Moire contrast in the local tunneling barrier height images of monolayer graphite on Pt(111), Phys. Rev. B 61 (2000) 15653–15656.
[36] Y. Yamada, A. Sinsarp, M. Sasaki, S. Yamamoto, Moire-like distribution of local tunneling barrier height of the monolayer graphite adsorbed on Pt(111) surface, Jpn. J. Appl. Phys. Part 1 41 (2002) 7501–7505.
[37] S.J. Altenburg, R. Berndt, Local work function and STM tip-induced distortion of graphene on Ir(111), New J. Phys. 16 (2014), 053036.
[38] W. Feng, S. Lei, Q. Li, A. Zhao, Periodically modulated electronic properties of the epitaxial monolayer graphene on Ru(0001), J. Phys. Chem. C 115 (2011) 24858–24864.
[39] S. Chen, M.H. von Hoegen, P.A. Thiel, M.C. Tringides, Diffraction paradox: an unusually broad diffraction background marks high quality graphene, Phys. Rev. B 100 (2019).
[40] S. Chen, M.H. von Hoegen, P.A. Thiel, A. Kaminski, B. Schrunk, T. Speliotis, et al., High layer uniformity of two-dimensional materials demonstrated surprisingly from broad features in surface electron diffraction, J. Phys. Chem. Lett. 11 (2020) 8937–8943.
[41] I. Pis, V. Stetsovych, J. Myslivecek, M. Kettner, M. Vondracek, F. Dvorak, et al., Atomic and electronic structure of V-Rh(110) near-surface alloy, J. Phys. Chem. C 117 (2013) 12679–12688.
[42] V. Joco, Universidad Autonoma de Madrid, PhD thesis, 2008.
[43] G.S. Tripathi, N.E. Brener, J. Callaway, Electronic-structure of rhodium, Phys. Rev. B 38 (1988) 10454–10462.
[44] A.K. Geim, K.S. Novoselov, The rise of graphene, Nat. Mater. 6 (2007) 183–191.
[45] P. Sutter, M.S. Hybertsen, J.T. Sadowski, E. Sutter, Electronic structure of few-layer epitaxial graphene on Ru(0001), Nano Lett. 9 (2009) 2654–2660.
[46] M. Kralj, I. Pletikosic, M. Petrovic, P. Pervan, M. Milun, A.T. N'Diaye, et al., Graphene on Ir(111) characterized by angle-resolved photoemission, Phys. Rev. B 84 (2011), 075427.
[47] H. Gonzalez-Herrero, P. Pou, J. Lobo-Checa, D. Fernandez-Torre, F. Craes, A. J. Martinez-Galera, et al., Graphene tunable transparency to tunneling electrons: a direct tool to measure the local coupling, ACS Nano 10 (2016) 5131–5144.
[48] B. Hammer, J.K. Norskov, Theoretical surface science and catalysis - calculations and concepts, in: B.C. Gates, H. Knozinger (Eds.), Advances in Catalysis, vol. 45, Impact of Surface Science on Catalysis, 2000, pp. 71–129.